Journal of
Materials Chemistry A

Materials for energy and sustainability

Accepted Manuscript

This article can be cited before page numbers have been issued, to do this please use: Q. Zou, B. Liu and Y. Zhang, *J. Mater. Chem. A*, 2023, DOI: 10.1039/D3TA02070C.

ROYAL SOCIETY OF CHEMISTRY

rsc.li/materials-a

View Article Online
DOI: 10.1039/D3TA02070C

Design of Array Structure for Carbon-based Field-Effect-Transistor Type Gas Sensor to Accurately Identify Trace Gas Species

Qiaoqiao Zou[1, a], Bin Liu[1, a], Yong Zhang[1, 2] *

[1] School of Physics and Optoelectronics, Xiangtan University, Xiangtan 411105, PR China.

[2] Hunan Institute of Advanced Sensing and Information Technology, Xiangtan University, Xiangtan 411105, PR China.

[a] These authors contributed equally to this work.

* Corresponding author. Tel: +86-0731-58293332.
E-mail address: zhangyong@xtu.edu.cn (Y. Zhang).

View Article Online
DOI: 10.1039/D3TA02070C

Highlight：

a) A carbon-based field effect transistor gas sensor with a gas-sensing gate is proposed to detect trace gas.

b) Using the noble metal nanoparticles/Co_3O_4 composites as the sensing gate ensures that the detection limit of gas sensor toward toluene is as low as 80 ppb.

c) A carbon-based field effect transistor sensor array with different gas sensing gates is designed to achieve accurate recognition of gas.

View Article Online
DOI: 10.1039/D3TA02070C

Abstract

The accurate identification of trace gases has become an important subject in the field of environmental monitoring due to the ppb-level permissible upper limit of indoor harmful gases. However, there are two challenges in trace gas detection, namely, the signal caused by the gas sensor is weak due to the extremely low concentration of trace gas, and the response signal of the target gas may be interfered by other gases owing to the crossing-sensitivity of materials. Herein, a carbon-based field effect transistor (FET) gas sensor array based on multi-sensing gates is presented. Based on the intrinsic amplifying effect of the field effect transistor, the proposed carbon-based FET-type gas sensor unit can detect the weak signal generated by 80 ppb gas at room temperature. Through the construction of the carbon-based FET gas sensor array structure with multi-sensing gates, the correlations between multiple parameters and gas species and concentrations are established, so as to realize the purpose of identifying the single unknown gas with an accuracy of 97.51%. This work provides a new strategy to develop micro gas sensor chips for accurate detection toward trace gases at room temperature.

Key words： Carbon-based FET gas sensor; Gas sensing gate; Gas sensor array; Trace gas detection; Gas identification

View Article Online
DOI: 10.1039/D3TA02070C

Introduction

Indoor volatile organic compounds (VOCs), which are released in large quantities by paint, cleaning products and furniture, seriously affect our health, causing severe diseases such as asthma, hearing loss and mental impairment [1-3]. According to the European air quality guidelines issued by the WHO, the upper allowable concentration of the indoor harmful gas is at the ppb level [4]. This means that the detection of trace gas has become an important research direction in the field of gas sensor. At present, the fundamental reason why trace gases are difficult to detect is that the electrical signal generated by trace gas molecules is too weak to be effectively captured due to too few adsorbed gas molecules on the sensing materials [2,5-7]. Moreover, the gas sensing property of the gas sensor is prone to interference from other gases in the environment, due to the similarity of the sensing mechanism between sensing materials and various gases [8,9]. And the sensing signal generated by a gas sensor is single, which makes it difficult to realize the comprehensive evaluation of gas species and concentrations. How to realize the effective amplification of weak signal caused by trace gases and how to improve the discrimination ability of gas sensor toward target gas become the key bottleneck issues to achieve accurate detection of trace target gas.

With the emergence of nanomaterials and the rapid development and application of semiconductor device manufacturing technology, the field effect transistor (FET) has attracted wide attention in the field of building highly sensing and integrated sensors because of its advantages such as high reliability, small size, good compatibility with CMOS technology and easy mass preparation [10-13]. In particular, the amplification

View Article Online
DOI: 10.1039/D3TA02070C

effect of the FET makes it easy for the FET-type gas sensor to capture the weak signal caused by the trace gas [5], which is expected to realize the effective detection of trace gas. Generally, for MOSFET, the carrier concentration in channel can be adjusted by the electrical signal on gate, and the excellent electrical property of the FET is the premise to ensure the effective amplification of weak signal on the gate of FET-type gas sensor [14], among which the channel material is one of the key factors determining the electrical performance of the FET [15-17]. At present, the information industrialization development of FETs has gradually entered the beyond-Moore era. According to relevant reports, semiconductor carbon nanotubes (CNTs) are considered to be very potential channel materials for the construction of the next generation FET because of their atomic thickness bodies, tunable bandgap and ultrahigh carrier mobility [18-23]. Moreover, compared with silicon-based FET, the preparation process of carbon-based FET is relatively simple [23], such as without the ion implantation process, which brings more development and opportunities for FET in the field of sensor.

In practical applications, it is difficult to accurately identify of gas concentration and species by a single gas sensor due to the strong cross-sensitivity of gas sensing materials. An effective strategy to construct a variety of signal parameters can be adopted to evaluate gas concentration and species [8]. Lu et al. effectively adjusted the selectivity of the sensor by introducing the noble metal nanoparticles (NMNPs) to modify In_2O_3 (NWs), and effectively and simultaneously distinguished different exhaled breath biomarkers by constructing a gas sensor array based on a variety of

View Article Online
DOI: 10.1039/D3TA02070C

NMNPs /In_2O_3 NWs [24]. The introduction of different NMNPs can effectively adjust the selectivity of the gas sensor toward the gas. Through the construction of the gas sensor array with different sensing gates, the various gas sensing parameters outputted by different gas sensor units can be obtained to comprehensively evaluate the concentration and species of gas [25-27]. However, the gas sensor array composed of multiple side-heating gas sensors has the disadvantages of large volume, overworking temperature and high-power consumption, which is unfavorable to the miniaturization development and portable application of gas sensors. Therefore, realizing the miniaturization and low power consumption of sensor array will benefit its application in the field of gas recognition.

In this work, CNTs are used as the channel of the FET device, and the wafer-scale preparation of the FET gas sensing platform is realized on a 4-inch wafer covered with random network CNTs. Through the inkjet printing technology and electron beam evaporation (EBE), a carbon-based FET gas sensor array is constructed by depositing different NMNPs/Co_3O_4 composites as sensing gates on carbon-based FET gas sensing platforms. Based on the amplification effect of FET, the gas sensor unit realizes the detection of toluene gas at ppb-level concentration. The identification of gas concentration and species is realized through the design of multi-sensing gates gas sensor array structure, which provides a new strategy for the development and application of sensor array in trace gas identification.

Experimental

View Article Online
DOI: 10.1039/D3TA02070C

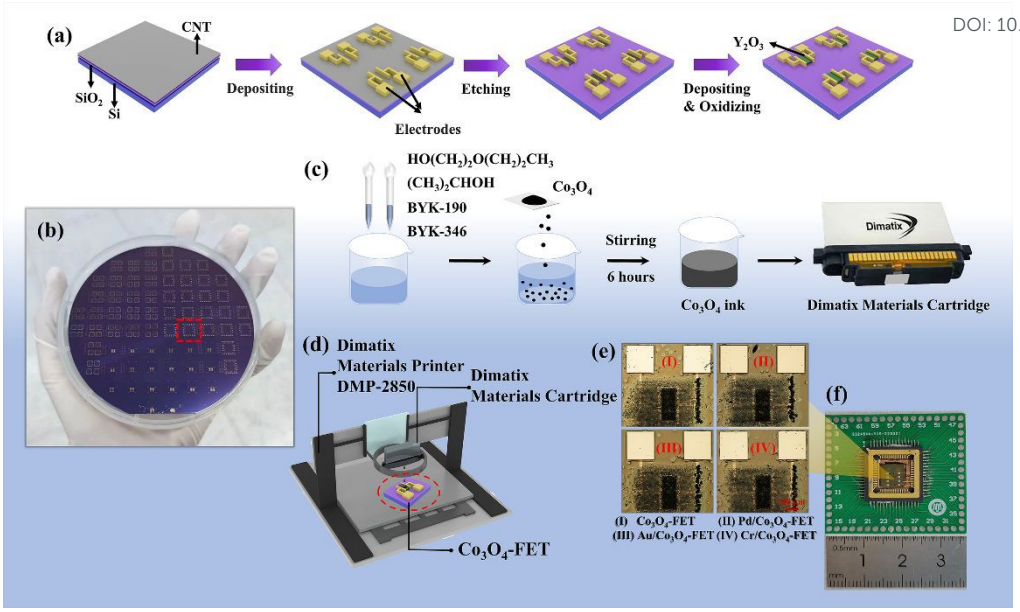

Fig. 1 (a) Fabrication process diagram of the carbon-based FETs. (b) Optical image of the wafer-scale devices array composed of FETs with various structures. Marked by the wire frame is the floating-gate FET gas sensing platform required for subsequent gas sensing experiments. (c) Configuration process diagram of the Co_3O_4 ink. (d) Diagram of the inkjet printing process, marked by the wire frame is the Co_3O_4-FET that is depositing the gate sensing layer. (e) Optical image of four kinds of floating-gate FET gas sensor units. (f) Photograph of the packaged sensor.

In this work, the carbon-based wafer is fabricated by coating the CNTs on a 4-inch Si/SiO_2 substrate to form a film by dip-coating method, and the detailed experimental procedures can refer to the work of Zhang's research team from Peking University [9,23]. The wafer-scale carbon-based FETs are fabricated by ultraviolet lithography (EVG 610, Austria), reactive ion etching (RIE, Haasrode-R200A, China) and EBE (DE400). The detailed fabrication process and optical images of the FET device are schematically illustrated in Fig. 1a. Firstly, the source (S) and Drain (D) electrode regions are defined on a 4-inch CNTs wafer by photolithography, and Ti/Pd/Au (0.3 nm/20 nm/40 nm) thin films are deposited by EBE at the rates of 0.1 Å/s, 1.0 Å/s and

View Article Online
DOI: 10.1039/D3TA02070C

1.0 Å/s, respectively. Secondly, in order to prevent the mutual interference between the sensors, the excess CNTs are etched under oxygen plasma for 60 s by photolithography and RIE to form a channel with a length of 300 μm and a width of 600 μm. An yttrium (Y) film with the thickness of 3 nm is deposited over the S/D electrode and channel by EBE at a low rate of 0.1 Å/s, and then thermally oxidized in air at 270°C for 30 min. Repeat the preceding operations one more time, an ultra-thin yttrium oxide (Y_2O_3) layer (thickness: ~12 nm, length: 800 μm, width: 1200 μm) is formed on the channel and S/D electrodes as the gate oxide layer of the FET. Finally, the wafer-scale devices array composed of FETs with various structures is successfully prepared by photolithography as shown in Fig. 1b, where the red wire frame area is the floating-gate FET gas sensing platform required for subsequent gas sensing experiments The size of a single FET device is 1.4 mm in width and 1.5 mm in length.

In order to be compatible with CMOS technology and realize mass preparation of sensors, the inkjet printing technology is used to uniformly and controllably deposit the sensing materials on the micron-sized floating-gate FET gas sensing platform [28-30]. In this work, the chemical reagents related to the preparation of inkjet printing ink are purchased from Aladdin Biochemical Technology Co., LTD. (Shanghai, China), and are not further purified. The preparation process diagram of the Co_3O_4 ink is shown in Fig. 1c. Firstly, 1.2 g Co_3O_4 nanoparticles (size: ~50 nm) is dissolved in the mixed solution composed of ethylene glycol propyl ether ($HO(CH_2)_2O(CH_2)_2CH_3$, 10 ml), isopropyl alcohol ($(CH_3)_2CHOH$, 10 ml), dispersive agent BYK-190 (1 ml) and organosilicone surfactant BYK-346 (1 ml). Then, the Co_3O_4 ink is obtained by magnetic

View Article Online
DOI: 10.1039/D3TA02070C

stirring at room temperature (~25℃) for 6 hours. After 2 ml Co_3O_4 ink is filled into the ink cartridge (Dimatix Materials Cartridge), a layer of Co_3O_4 film is printed on the gate region exposed in advance by lithography of the prepared floating-gate FET gas sensing platform by the materials printer (Model: DMP-2850, Fujifilm, America, Substrate temperature: 50℃, Drop spacing: 25 μm, Drop volume: 10 pL, Print time: once) as shown in Fig. 1d , then the deposited film is annealed on a heater at 200℃ for 15 min to form a gas sensing gate, and finally the carbon-based FET Co_3O_4 gas sensor is obtained as shown in Fig. 1e (Ⅲ). In addition, in order to construct a floating-gate FET gas sensor array with multiple sensing gates, Pd, Au and Cr nanoparticles with a thickness of 1 nm are deposited respectively at the rate of 0.1 Å/s on the surface of Co_3O_4 by EBE to prepare four kinds of floating-gate FET gas sensor units as shown in Fig. 1e, which are defined as (Ⅰ) Co_3O_4-FET, (Ⅱ) Pd/Co_3O_4-FET, (Ⅲ) Au/Co_3O_4-FET and (Ⅳ) Cr/Co_3O_4-FET, respectively. In order to prevent the sensor from being contaminated by dust in the air, the prepared sensors are packaged on the self-made printed circuit board through wire bonding, as shown in Fig. 1f.

Ultraviolet-Visible-near-infrared spectroscopy (UV-3600, Shimadzu, Japan) and Raman spectroscopy (Renishaw in Via, UK) are performed to verify the purity of the CNTs film. The surface morphologies of CNTs film and sensing materials are investigated by field emission scanning electron microscopy (FE-SEM, Hitachi SU5000, Japan). The material compositions of sensing materials are characterized by X-ray photoelectron spectroscopy (XPS, Thermo ESCALAB 250Xi). The electrical properties of the floating-gate FET gas sensors are measured using a Keithly 4200

View Article Online
DOI: 10.1039/D3TA02070C

semiconductor analyzer combined with a probe stand (Cascade Microtech MPS 150). As shown in Fig. S1a, the gas sensing measurement platform is composed of DGL-Ⅲ humidity control gas-liquid distribution system, test chamber, and CGS-MT intelligent gas-sensing analysis system (Beijing Elite Tech Co., Ltd., China). Fig. S1b exhibits the corresponding digital photo. The gases required for the gas sensing test are purchased from Dalian Special Gas Co., Ltd. (Dalian, China) and calibrated with the Fourier Transform infrared spectrometer (Spectrum 100). The MFC1 (maximum flow rate: 1000 sccm) and MFC2 (maximum flow rate: 100 sccm) of the DGL-Ⅲ are used to control the flow rate of the air and the high concentration target gas, respectively, to synthesize the target gas (C_7H_8, HCHO, C_6H_6, NH_3, NO_2) with different concentrations required by the experiment. The Response is defined as the Response = $\frac{I_g - I_a}{I_a} \times 100\%$, where I_g and I_a are the currents of the sensor in the target gas and air, respectively [31]. The response and recovery times are expressed as the time required for the gas sensing current change to reach 90% of the total current change [32].

Results & Discussion

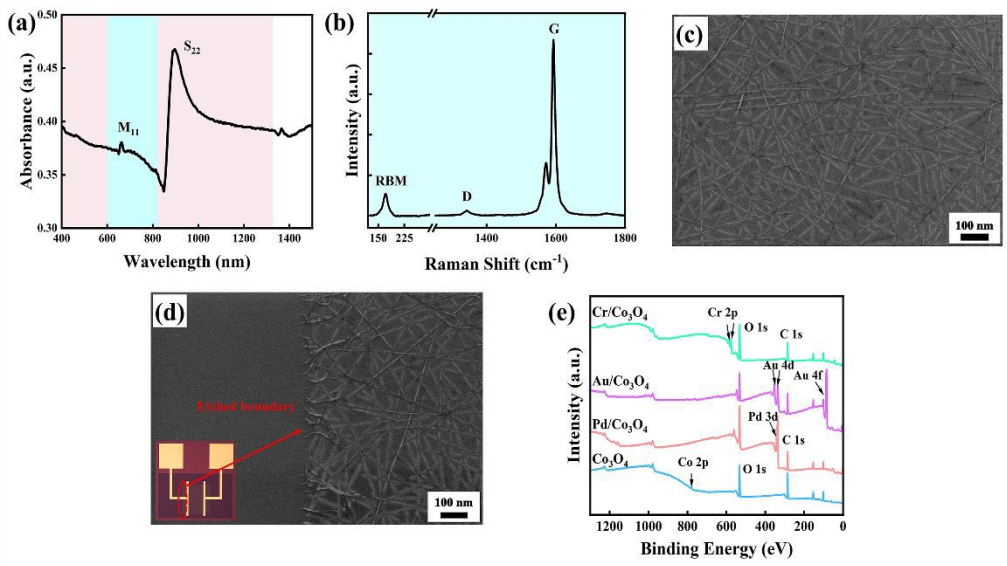

View Article Online
DOI: 10.1039/D3TA02070C

Fig. 2 (a) UV–vis–NIR absorption spectra and (b) Raman spectra of the CNTs film. FE-SEM images of (c) the CNTs film and (d) the channel region after etching. (e) Full XPS spectra of Co_3O_4, Pd/Co_3O_4, Au/Co_3O_4 and Cr/Co_3O_4.

It is well known that the high-quality channel material is the key to the construction of FET with good electrical property [23,33]. Therefore, a series of characterizations of CNTs films of floating-gate FET are firstly carried out, as shown in Fig.2. Fig. 2a exhibits the absorption spectra of the CNTs film in the range of 400-1500 nm. The peaks of M_{11} and S_{22} can be observed at 600-800 nm and 820-1350 nm, respectively. The characteristic peaks of M_{11} and S_{22} indicate the existence of metallic and semiconductor fractions in CNTs, respectively. Compared with the weak M_{11} peak, the intensity of the S_{22} peak is much stronger, indicating the high semiconducting purity of the CNTs [34-37]. In order to further characterize the quality of CNTs film, the Raman spectra of CNTs film is obtained, as shown in Fig. 2b. The peaks D and G at 1340 and ~1590 cm^{-1} are the typical Raman characteristic peaks of the CNTs [38]. The higher I_G/I_D ratio indicates that the CNTs used in this work have fewer defects [39,40], which ensures the good electrical properties of the FET, such as high carrier mobility [41,42]. In addition, it can be seen from Fig. 2b that a radial respiration mode (RBM) peak appears at 170 cm^{-1} [43]. According to the experimental relationship of $\omega = 248/d$ (nm) (ω and d are the RBM Raman shift and the CNTs diameter, respectively), the diameter of the CNTs is distributed around 1.5 nm [39], which is shown that the thickness of the channel composed of CNTs is in atomic dimension. Fig. 2c shows the FE-SEM image of the carbon-based wafer. The CNTs are distributed uniformly and densely in a random

View Article Online
DOI: 10.1039/D3TA02070C

network on the Si/SiO_2 substrate, which means that the carbon-based FET can be prepared on the CNTs wafer without positioning, providing the support for the preparation of the wafer-scale carbon-based FETs. The FE-SEM image of the CNTs channel boundary etched by reactive ion etching is shown in the Fig. 2d. A sharp boundary can be observed between the channel region and the etched region. After the etching process, the left etched region is very clean without residual CNTs, and the CNTs in the right channel region are not affected, indicating that the channel region is formed successfully by a controllable and accurate etching process.

In order to characterize the elemental composition and chemical state of the materials, the surface chemical analyses of Co_3O_4 and three NMNPs/Co_3O_4 materials composites are performed by XPS. Fig. 2e exhibits the full XPS spectra of Co_3O_4 and Pd, Au and Cr modified Co_3O_4, Pd/Co_3O_4, Au/Co_3O_4 and Cr/Co_3O_4 contain Pd, Au and Cr peaks respectively in addition to the peaks of Co, O and C in Co_3O_4, confirming the successful modification of the three NMNPs, where all binding energy values in the XPS spectra are calibrated with a peak of C 1s (284.8 eV). Fig. S2 depicts the high-resolution XPS spectra of Pd 3d, Au 4f and Cr 2p respectively, which is used to determine the valence states of Pd, Cr and Au. The XPS high-resolution spectra of Pd 3d are of three peaks, which are related to Pd $3d_{3/2}$ and Pd $3d_{5/2}$, respectively. The double peaks fitted by Pd $3d_{5/2}$ are located at 336.1eV and 337.9eV, corresponding to Pd^{2+} and Pd^0, respectively [44]. The presence of Pd^{2+} indicates the presence of PdO in the Pd/Co_3O_4, but the amount is rarely negligible [45-47]. The two peaks of Au 4f at 88.1 eV and 84.42 eV correspond to Au $4f_{5/2}$ and Au $4f_{7/2}$ states, and the two peaks of Cr 2p

View Article Online
DOI: 10.1039/D3TA02070C

at 586.6eV and 577 eV belong to Cr $2p_{1/2}$ and Cr $2p_{3/2}$, respectively. The binding energy differences between the peaks of Au 4f and Cr 2p are 5.3 eV and 3.78 eV, respectively, confirming that the Au and Cr nanoparticles are not oxidized. These features are consistent with the binding energies of metallic Au and Cr reported in the literature [48-51].

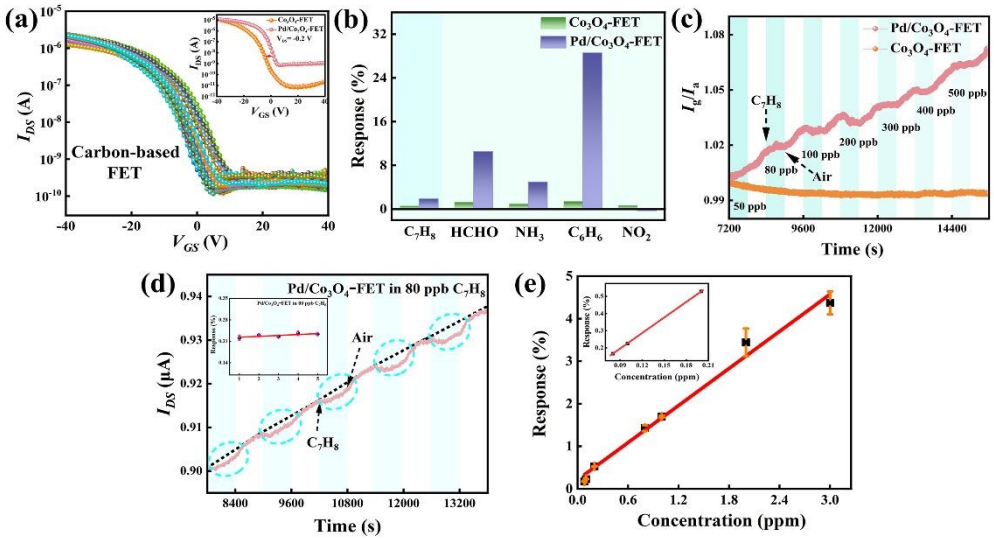

Fig. 3 (a) Transfer characteristic curves of the carbon-based FET, the inset is the transfer characteristic curves of the Co_3O_4-FET and Pd/Co_3O_4-FET, respectively. (b) Comparison of response values of the Co_3O_4-FET and Pd/Co_3O_4-FET to different gases. (c) Dynamic response/recovery curves of the Co_3O_4-FET and Pd/Co_3O_4-FET at the range of 50-500 ppb C_7H_8. (d) Dynamic response curves of the Pd/Co_3O_4-FET at 80 ppb C_7H_8 for five cycles, and the marked wire frames correspond to the five responses. The inset shows the corresponding response values. (e) Response fitting curve of Pd/Co_3O_4-FET to C_7H_8 at the range of 50 ppb-3 ppm.

As a gas sensing platform, the FET should be fabricated with high yield, reliability, and performance uniformity. The transfer characteristic curves of the carbon-based FETs are tested at the V_{GS} range from -40 to +40 V and the V_{DS} of -0.2 V. There is no

View Article Online
DOI: 10.1039/D3TA02070C

significant difference in the transfer characteristic curves of randomly selected fifty-five carbon-based FETs, indicating that the wafer-scale carbon-based FETs are highly consistent. All transistors present p-channel depletion FETs, and the current on/off ratios of the transistors are ~10^4. The inset of Fig. 3a shows the transfer characteristic curves of Co_3O_4-FET and Pd/Co_3O_4-FET gas sensors, respectively. Compared with the carbon-based FET, the transfer characteristic curve of Co_3O_4-FET is changed due to the changes in the gate oxide layer capacitance of the FET caused by deposition of gate sensing layer [52]. After the deposition of Pd nanoparticles, the transfer characteristic curve of the Co_3O_4-FET is obviously shifted and the current on/off ratio decreases significantly. This phenomenon is due to the fact that Pd (5.59 eV) [53] is a high-work-function metal and its deposition changes the work function of the gate sensing material, leading to the change in the surface potential and thus changing the threshold voltage of the sensor [54]. As shown in the inset of Fig. 3a, when the gate voltage is 0 V, the carbon-based FET gas sensors are in the on-state, which means that the carbon-based FET sensors can operate without gate voltage, reducing energy consumption.

Then, the gas sensing property of the gas sensor is detected. In order to avoid the influence of the environment on the experimental results, the subsequent gas sensing performance experiments are carried out at room temperature with the relative humidity (RH) of 0.4%RH in the test chamber. It is well known that selectivity is one of the performance evaluation parameters of gas sensor in practical application. The gas sensing response values of Co_3O_4-FET and Pd/Co_3O_4-FET are tested in different gases (HCHO, C_7H_8, NH_3, NO_2 and C_6H_6) at 3 ppm. As shown in Fig. 3b, the Co_3O_4-FET

View Article Online
DOI: 10.1039/D3TA02070C

presents similar weak responses to all gases, making it difficult to distinguish the species of gases. After the introduction of the Pd NMNPs, except for the oxidizing gas NO_2 (almost no response), the responses of the Pd/Co_3O_4-FET to reducing gases HCHO, NH_3, C_7H_8 and C_6H_6 are improved to varying degrees. Among them, and the response of the Pd/Co_3O_4-FET to C_7H_8 is the weakest at the same concentration. In order to prove the ability of FET-type gas sensor to detect trace gases at room temperature, C_7H_8, with the weakest response of the gas sensor, is selected as an example to detect, and analyze its gas sensitivity mechanism. In order to confirm that the gas sensing properties of subsequent experiments are mainly from the gate sensing materials, the dynamic response/recovery curves of carbon-based FET with and without Co_3O_4 sensing layer exposed to C_7H_8 at 3 ppm are tested, as shown in Fig. S3. It can be seen that, when switching from air to C_7H_8, the I_{DS} of the carbon-based FET changes little, while the I_{DS} of the Co_3O_4-FET increases gradually, and decreases with Co_3O_4-FET switching to air environment, confirming that the carbon-based FET does not respond to C_7H_8 and all subsequent gas sensing responses come from the gate sensing materials. In order to evaluate the detection capability of the carbon-based FET-type gas sensor for C_7H_8 at the ppb level, the dynamic response/recovery curves of Co_3O_4-FET and Pd/Co_3O_4-FET towards C_7H_8 at the concentrations of 50-500 ppb are tested, as shown in Fig. 3c. At the room temperature, the I_{DS} of the Co_3O_4-FET exposed to C_7H_8 at the ppb-level concentration does not change significantly, indicating that the Co_3O_4-FET is difficult to detect trace C_7H_8, while the Pd/Co_3O_4-FET shows an obvious gas sensing response to C_7H_8 at 80 ppb, which meets the maximum allowable concentration standard of C_7H_8

View Article Online
DOI: 10.1039/D3TA02070C

issued by WHO [55].

Fig. 3d further shows the dynamic response/recovery curve of the Pd/Co_3O_4-FET at 80 ppb C_7H_8 for 5 cycles. The marked wire frames correspond to five responses respectively, and the corresponding response values are shown in the inset. As can be seen from Figure 3d, baseline drift exists in the dynamic response/recovery curve. This phenomenon is caused by the fact that there is not enough desorption energy at room temperature for C_7H_8 molecules to be desorbed from the surface of the gas-sensing materials. However, it should be pointed out that the change of the I_{DS} caused by each injection of 80 ppb target gas to the Pd/Co_3O_4-FET is consistent. It can be seen from the inset of Fig. 3d that the Pd/Co_3O_4-FET has basically the same response values to C_7H_8 at the same concentration, which means that the baseline drift will not affect the judgment of the gas sensor's gas-sensing response, and indicates that the Pd/Co_3O_4-FET has good repeatability of trace gas detection. According to the response fitting curve shown in Fig. 3e, the response of Pd/Co_3O_4-FET to C_7H_8 gas increases linearly with the increase of gas concentration. Especially, the response of the sensor to C_7H_8 can be proportional to the gas concentration within the concentration variation range of ppb-level. In addition, Fig. S4 shows relatively stable response signals of the Pd/Co_3O_4-FET exposed to 2 ppm C_7H_8 for 20 days. The error of the ten response signals is 5.24%, indicating that the gas sensor Pd/Co_3O_4-FET has good long-term stability. In order to better exhibit the excellent capability of the Pd/Co_3O_4-FET for trace gas detection, the gas-sensing response of the Pd/Co_3O_4-FET to C_7H_8 (with the weakest response) is statistically compared with other reported C_7H_8 gas sensors based on different gas-

View Article Online
DOI: 10.1039/D3TA02070C

sensing materials [56-60], as shown in Table S1. It can be seen that the Pd/Co_3O_4-FET in this work can realize the detection limit of 80 ppb for C_7H_8 at room temperature, which is far lower than that of other gas sensors, which confirms that it is a very good strategy for trace gas detection based on the amplification effect of FET.

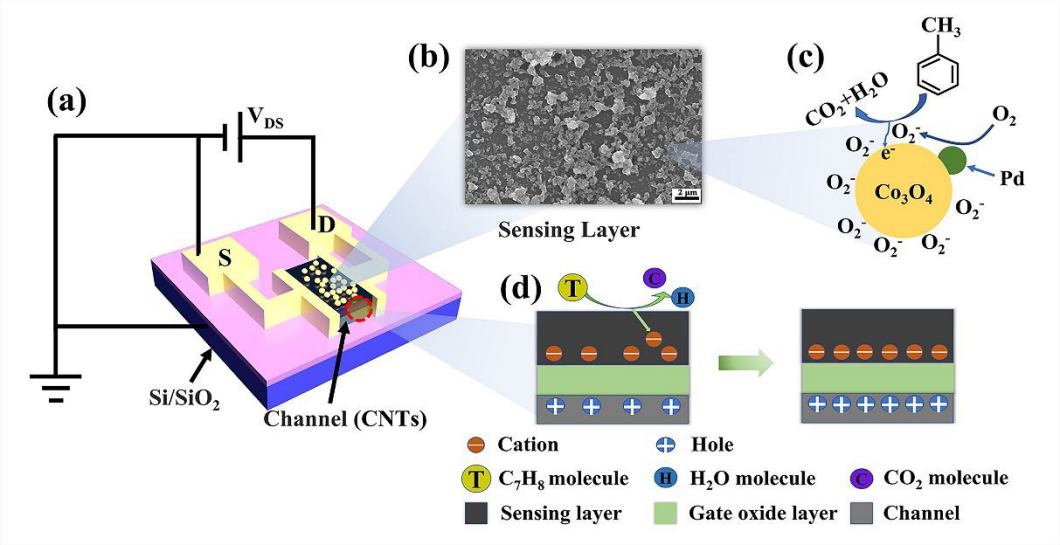

Fig. 4 (a) Test circuit diagram for gas sensing test of the Pd/Co_3O_4-FET sensor. (b) FE-SEM image of sensing material deposited on the gate area of Pd/Co_3O_4-FET sensor. The sensing mechanism diagram of the (c) the gas sensing material and (d) the gas sensor.

Through the amplification effect of the carbon-based FET and the introduction of the NMNPs Pd, the Pd/Co_3O_4-FET can detect toluene gas as low as 80 ppb, and the gas sensing mechanism of the Pd/Co_3O_4-FET is discussed in detail as follows. Fig. 4a exhibits the schematic diagram of the operating circuit of the Pd/Co_3O_4-FET for gas sensing test. In this work, a carbon-based FET gas sensor with the floating gate is prepared. High-purity semiconductor CNTs are used as the channel materials to provide a high-speed electronic transport channel for the carbon-based FET gas sensor [33]. The gate oxide layer covered on the CNTs separates the channel transport layer from

View Article Online
DOI: 10.1039/D3TA02070C

the gate sensing layer so that they can give full play to their respective advantages and form a gas sensor integrating gas detection and signal amplification, which is the main reason for the low detection limit of the gas sensor [10]. The sensing layer deposited on the gate oxide layer is used to realize the gas sensing function. Fig. 4b shows the FE-SEM morphology of the Pd/Co_3O_4 sensing layer. It can be seen that the sensing materials prepared by inkjet printing are uniformly and discretely distributed on the gate oxide layer of the FET. The discontinuity of the sensing materials avoids the possibility that the sensing gate of the FET cannot regulate the channel current due to the short-circuiting of the S/D electrodes. It is also conducive to the gas molecules acting on the three-phase boundaries formed by the gate sensing materials and the gate oxide layer to regulate the channel current of the FET sensor [61,62].

As a catalytic metal, Pd nanoparticles have high availability to catalyze the dissociation of molecular oxygen into active oxygen ions. At room temperature, when Pd/Co_3O_4-FET is placed in the air, lots of oxygen molecules are adsorbed on the surface of the sensing materials and catalyzed to decompose into active oxygen ions O_2^- (the adsorbed oxygen type is determined by working temperature ~25 ℃) [63,64] while capturing electrons of the sensing materials (Fig. 4c) [65,66]. As shown in Fig. 4d, when the Pd/Co_3O_4-FET is exposed to C_7H_8 environment, the trace C_7H_8 gas molecules are catalyzed into small molecules by a large number of active oxygen ions on the surface of Co_3O_4 and the electrons are released [67], which increases the number of the electrons at the interface between the sensing materials and the gate oxide layer. The Pd/Co_3O_4-FET in this work is a P-type FET sensor whose channel current mainly

View Article Online
DOI: 10.1039/D3TA02070C

depends on holes, and the holes in the channel are induced to the channel surface due to the interaction between dipoles, reducing the concentration of holes for conduction [68,69]. The decrease of the holes in the channel reduces the I_{DS} of the gas sensor, which is consistent with the response behavior of the Pd/Co_3O_4-FET to toluene in the above experiments.

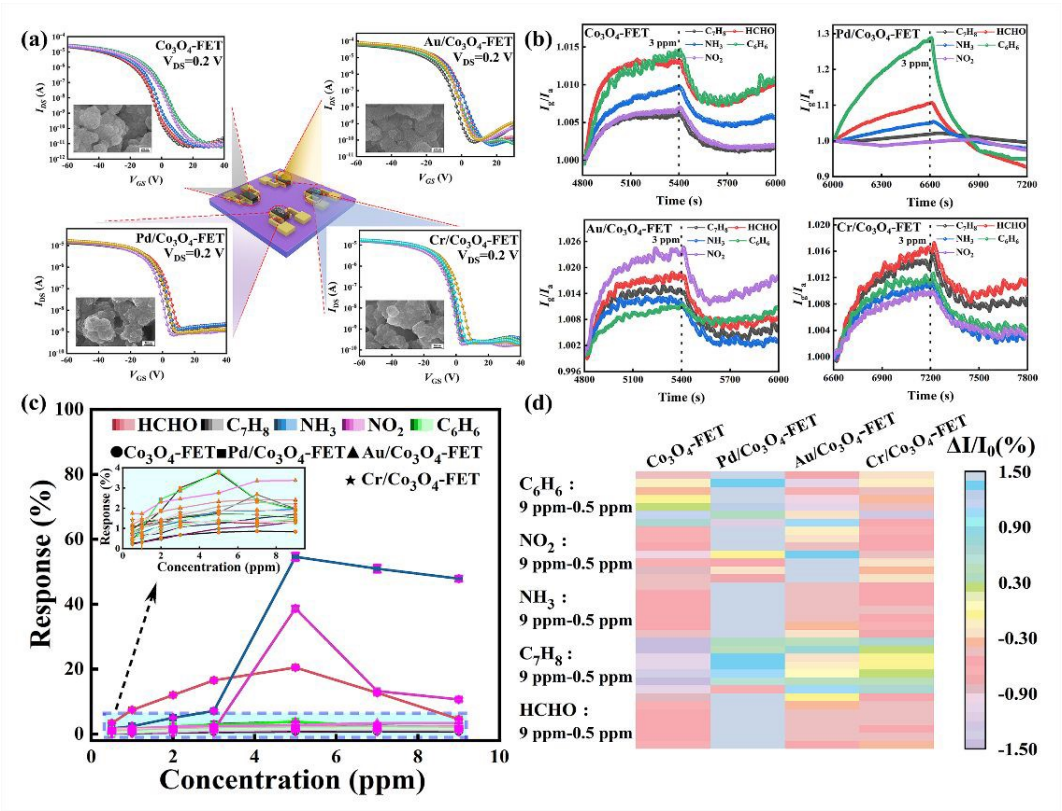

Fig. 5 (a) Transfer characteristic curves of the four gas sensor units, respectively. The inserts are the surface topographies of the sensing materials corresponding to the sensors, respectively. (b) Responses of the four gas sensor units to the five kinds of gases at 3 ppm. (c) Response value curves of the four gas sensor units to the five kinds of gases at the range of 0.5-9 ppm. (d) Response heat maps of the four gas sensor units gas sensors to the five kinds of gases.

It is noteworthy that the modification of the NMNPs Pd changes the selectivity of the Co_3O_4-FET, which gives us an inspiration that the modifications of different

View Article Online
DOI: 10.1039/D3TA02070C

NMNPs to the sensing materials are expected to regulate the selectivity of the gas sensor to different gases. Therefore, two other NMNPs, i.e., Au and Cr, are introduced to prepare Au/Co_3O_4-FET and Cr/Co_3O_4-FET, and a carbon-based FET gas sensor array composed of Co_3O_4-FET, Pd/Co_3O_4-FET, Au/Co_3O_4-FET and Cr/Co_3O_4-FET is constructed to comprehensively evaluate the species and concentrations of gases. In order to ensure the consistency of the same gas sensor unit after the metal modification, the transfer characteristic curves of these four kinds of gas sensor units are tested respectively, as shown in Fig. 5a. The insets show the surface topographies of the sensing materials corresponding to the sensors, respectively. It can be seen that the gas sensor units with different modified metals have different transfer characteristic curves due to different work functions of the modified metal, but the same kind of sensors have good consistency. The comparison of dynamic response/recovery curves of the four gas sensor units to five gases at 3 ppm at the same V_{DS} is shown in Fig. 5b. A detailed comparison of the response values is shown in Table S2. It can be seen that the response values of the four gas sensor units to the five gases are significantly different. The Co_3O_4-FET shows similar response to the five gases, while Pd/Co_3O_4-FET, Au/Co_3O_4-FET and Cr/Co_3O_4-FET show different degrees of higher responses to C_6H_6, NO_2 and HCHO, respectively. It is shown that the modifications of different NMNPs change the gas sensing responses of the gas sensor to different gases. The dynamic response/recovery curves of four gas sensor units to 0.5-9 ppm gases (HCHO, C_7H_8, NH_3, NO_2 and C_6H_6) are further tested, as shown in Fig. S5. Based on data in Fig. S5, 20 response curves of the four gas sensor units to the five gases of different

View Article Online
DOI: 10.1039/D3TA02070C

concentrations are obtained, as shown in Fig. 5c. The response of the gas sensor array to the five gases is obviously different at high concentration. However, due to the great difference in the response of the gas sensor array at the high concentration and low concentration gases, the response curves of that at low concentration coincide. But as can be seen in the inset, the gas sensor array also responds significantly differently to low concentrations of the five gases. In order to more intuitively observe and analyze the response of the gas sensor array to the five gases at different concentrations, a visual response heat map (Fig. 5d) is drawn according to the corresponding response signals in Fig. 5c.

Based on the experimental data, the correlations between the multiple gas-sensing parameters and gas species and concentrations are established, and an identification strategy are proposed. When the gas sensor array is exposed to gas Gx of unknown species (the range of the species: HCHO, C_7H_8, NH_3, NO_2, and C_6H_6) and unknown concentration (concentration range: 50 ppb-9 ppm), the four gas sensor units respectively output four response signals s1, s2, s3 and s4, and locate the distribution position of the four response signals in Fig. 5d, corresponding to the specific gas species and concentration. In order to verify the feasibility of the gas identification strategy, the gas sensor array is exposed to gas sample of unknown species and concentration, and obtain the corresponding response values of the four gas sensor units of the gas sensor array, as shown in Fig. S6. Through positioning and comparison, the test sample data is verified. Although the response values of the Pd/Co_3O_4-FET are slightly different, the response values of the Co_3O_4-FET, Au/Co_3O_4-FET and Cr/Co_3O_4-FET are

View Article Online
DOI: 10.1039/D3TA02070C

consistent with the database samples, comprehensively evaluating and determining the unknown gas as 2 ppm C_6H_6. This recognition strategy can eliminate the interference of other gases to realize the accurate recognition of a single unknown gas, and the recognition accuracy of gas is up to 97.51%.

Conclusions

To sum up, in this work, the CNTs are used as the channel material of FET, and the wafer-scale carbon-based FETs are prepared on the substrate covered by a random network arrangement of CNTs by micro-nano fabrication technology. Based on the inkjet printing technology, a variety of the NMNPs/Co_3O_4 composite are prepared on the floating-gate FETs as sensing gates, and a floating-gate FET gas sensor array based on multi-sensing gates is constructed. Based on the inherent amplification effect of the FET, the detection limit of the Pd/Co_3O_4-FET to gas at room temperature is as low as 80 ppb, and the gas sensor has better sensitivity and repeatability. In addition, different NMNPs are introduced to adjust the selectivity of the gas sensor, and the correlations between multiple parameters produced by different gas sensor array units and gas species and concentrations are established. The identification accuracy of C_7H_8, C_6H_6, HCHO, NH_3 and NO_2 is achieved with 97.51%. This work provides a new solution for the design of micro-integrated gas sensor array chip which has the ability of trace gas detection and high gas recognition.

View Article Online
DOI: 10.1039/D3TA02070C

Author Contributions (optional)

Qiaoqiao Zou: Methodology, Formal analysis, Investigation, Resources, Data Curation, Writing - Original Draft, Visualization. **Bin Liu:** Writing - Review & Editing. **Yong Zhang:** Conceptualization, Supervision, Conceptualization, Project administration, Funding acquisition.

Conflicts of interest

The authors declare that they have no conflict of interest.

Acknowledgments

This work was supported by National Natural Science Foundation of China (62071410, 62101477) and Hunan Provincial Natural Science Foundation (2021JJ40542).

View Article Online
DOI: 10.1039/D3TA02070C

References

[1] World Health Organization. Regional Office for Europe. (2010). WHO guidelines for indoor air quality: selected pollutants. World Health Organization. Regional Office for Europe. https://apps.who.int/iris/handle/10665/260127

[2] Kim K.B., Jeong S.-Y., Kim T.-H., Kang Y.C., Lee J.-H. Methylbenzene sensors using Ti-doped NiO multiroom spheres: versatile tunability on selectivity, response, sensitivity, and detection limit, Sens. Actuators B Chem. 2020, 308, 127730.

[3] Rumchev K., Spickett J., Bulsara M., Phillips M., Stick S. Association of Domestic Exposure to Volatile Organic Compounds with Asthma in Young Children. Asthma 2004, 59, 746−751.

[4] World Health Organization. Regional Office for Europe. (2000). Air quality guidelines for Europe, 2nd ed. World Health Organization. Regional Office for Europe. https://apps.who.int/iris/handle/10665/107335

[5] Zhou X., Wang Y., Wang J., Xie Z., Wu X., Han N., Chen Y. Amplifying the Signal of Metal Oxide Gas Sensors for Low Concentration Gas Detection. IEEE Sensors Journal 2017, 17, 2841–2847.

[6] Woellner M., Hausdorf S., Klein N., Mueller P., Smith M.W., Kaskel S. Adsorption and Detection of Hazardous Trace Gases by Metal-Organic Frameworks. Advanced Materials 2018, 30, 1704679.

[7] Amico A. D., Marcellis A. De., Carlo C. Di., Natale C. Di., Ferri G., Martinelli E., Paolesse R., Stornelli V. Low-voltage low-power integrated analog lock-in amplifier for gas sensor applications, Sensors B: Chem. 2010, 144, 400–406.

[8] Raj V.B., Nimal A.T., Parmar Y., Sharma M.U., Sreenivas K., Gupta V. Cross-sensitivity and selectivity studies on ZnO surface acoustic wave ammonia sensor, Sens. Actuators B Chem. 2010, 147, 517–524.

[9] Ree J., Kim Y. H., Shin H. K. Dynamics of gas-surface interactions: Reaction of atomic oxygen with chemisorbed hydrogen on Tungsten. J. Phys. Chem. A. 1997, 101, 25, 4523-4534.

[10] Liang Y., Xiao M., Wu D., Lin Y., Liu L., He J., Zhang G., Peng L.-M., Zhang Z. Wafer-Scale Uniform Carbon Nanotube Transistors for Ultrasensitive and Label-Free Detection of Disease Biomarkers. ACS Nano 2020, 14, 8866–8874.

[11] Jin H., Yu J. K., Cui D. X., Gao S., Yang H., Zhang X. W., Hua C. Z., Cui S. S., Xue C. L., Zhang Y. A., Zhou Y., Liu B., Shen W. F., Deng S. W., Kam W. L., Cheung W. F. Remote Tracking

View Article Online
DOI: 10.1039/D3TA02070C

Gas Molecular via the Standalone-Like Nanosensor-based Tele-Monitoring System. Nano-Micro Lett. 2021, 13, 1–14.

[12] Wada T., Murata N., Suzuki T., Uehara H., Nitani H., Niwa Y., Uo M., Asakura K. Improvement of a Real Gas-Sensor for the Origin of Methane Selectivity Degradation by μ-XAFS Investigation. Nano-Micro Lett. 2015, 7, 255– 260.

[13] Grassi M., Malcovati P., Baschirotto A. A 141-dB dynamic range CMOS gas-sensor interface circuit without calibration with 16-bit digital output word. IEEE J. Solid-State Circ. 2007, 42, 1543-1554

[14] Lundström I., Shivaraman S., Svensson C., Lundkvist L. A hydrogen-sensitive MOS field-effect transistor Appl. Phys. Lett. 1975, 26, 55-57.

[15] Ogawa K., Kato T., Ikegami A., Tsuji H., Aoki N., Ochiai Y., Bird J.P. Electrical properties of field-effect transistors based on C_{60} nanowhiskers. Applied Physics Letters. 2006, 88, 112109.

[16] Mukherjee A., Rosenwaks Y. Recent Advances in Silicon FET Devices for Gas and Volatile Organic Compound Sensing. Chemosensors. 2021, 9, 260.

[17] Franklin A. D. Nanomaterials in transistors: From high-performance to thin-film applications. Science, 2015, 349, 704.

[18] Cao Q., Kim H.-S., Pimparkar N., Kulkarni J.P., Wang C., Shim M., Roy K., Alam M.A., Rogers J.A. Medium-scale carbon nanotube thin-film integrated circuits on flexible plastic substrates. Nature. 2008, 454, 495–500.

[19] Gu J., Han J., Liu D., Yu X., Kang L., Qiu S., Jin H., Li H., Li Q., Zhang J. Solution-Processable High-Purity Semiconducting SWCNTs for Large-Area Fabrication of High-Performance Thin-Film Transistors. Small. 2016, 12, 4993−4999.

[20] Liu L., Han J., Xu L., Zhou J. S., Zhao C. Y., Ding S. J., Shi H. W., Xiao M. M., Ding L., Ma Z., Jin C. H., Zhang Z. Y., Peng L. M. Aligned, High-density Semiconducting Carbon Nanotube Arrays for High-performance Electronics. Science. 2020, 368, 850– 856.

[21] Xia F., Xia T., Xiang L., Liu F., Jia W.J., Liang X.L., Hu Y.F. High-Performance Carbon Nanotube-Based Transient Complementary Electronics. ACS Appl. Mater. 2022, 14, 10, 12515-12522.

[22] Wang T., Huang D., Yang Z., Xu S. S., He G. L., Li X. L., Hu N. T., Yin G. L., He D. N., Zhang L. Y. A Review on Graphene-based Gas/Vapor Sensors with Unique Properties and Potential Applications. Nano-Micro Lett. 2016, 8, 95–119.

[23] Star A., Han T.-R., Joshi V., Gabriel J.-C.P., Grüner G. Nanoelectronic Carbon Dioxide Sensors. Adv. Mater. 2004, 16, 2049–2052.

[24] Liu W., Sun J., Xu Lin., Zhu S.D., Zhou X.Y., Yang S., Dong B., Bai X., Lu G.Y., Song H.W. Understanding the noble metal modifying effect on In_2O_3 nanowires: highly sensitive and selective gas sensors for potential early screening of multiple diseases. Nanoscale Horiz. 2019, 4, 1361-1371.

[25] Walt D.R. Electronic Noses: Wake Up and Smell the Coffee. Anal. Chem. 2005, 77, 45A–45A.

[26] Shi L., Tang Q., Yang B., Liu W., Li B., Yang C., Jin Y. Portable and Label-Free Sensor Array for Discriminating Multiple Analytes via a Handheld Gas Pressure Meter. Anal. Chem. 2022, 94, 14453–14459.

[27] Shi L., Liu J., Li B., Yang B. X., Jin C. Y., Jin Y. Multichannel Paper Chip-Based Gas Pressure Bioassay for Simultaneous Detection of Multiple MicroRNAs. ACS Appl. Mater. Interfaces. 2021, 13, 15008– 15016.

[28] Zhang Z., Zhang X., Xin Z., Deng M., Wen Y., Song Y. Synthesis of monodisperse silver nanoparticles for ink-jet printed flexible electronics. Nanotechnology. 2011, 22, 425601.

[29] Lin Y., Chen J., Tavakoli M.M., Gao Y., Zhu Y., Zhang D., Kam M., He Z., Fan Z. Printable Fabrication of a Fully Integrated and Self-Powered Sensor System on Plastic Substrates. Adv. Mater. 2019, 31, 1804285.

[30] Peng X., Liu J., Tan Y., Mo R., Zhang Y. A CuO thin film type sensor via inkjet printing technology with high reproducibility for ppb-level formaldehyde detection, Sens. Actuat. B: Chem. 2022, 362, 131775.

[31] He Q., Zeng Z., Yin Z., Li H., Wu S., Huang X., Zhang H. Fabrication of flexible MoS_2 thin-film transistor arrays for practical gas-sensing applications Small. 2012, 8, 2994-2999.

[32] Casals O., Markiewicz N., Fabrega C., Gracia I., Cané C., Wasisto H. S., Waag A., Prades J. D. A Parts Per Billion (ppb) Sensor for NO_2 with Microwatt (muW) Power Requirements Based on Micro Light Plates. ACS Sens. 2019, 4, 822−826.

[33] Liu C., Hu J., Wu G., Cao J., Zhang Z., Zhang Y. Carbon Nanotube-Based Field-Effect Transistor-Type Sensor with a Sensing Gate for Ppb-Level Formaldehyde Detection. ACS Appl. Mater. 2021, 13, 56309–56319.

[34] Zhou C., Zhao J., Ye J., Tange M., Zhang X., Xu W. Printed thin-film transistors and NO_2 gas sensors based on sorted semiconducting carbon nanotubes by isoindigo-based copolymer, Carbon. 2016, 108, 372–380.

[35] Kong J., Franklin N. R., Zhou C. W., Chapline M. G., Peng S., Cho K. J., Dai H. J. Nanotube Molecular Wires as Chemical Sensors. Science. 2000, 287, 622– 625.

[36] Zhong D., Zhang Z. Y., Ding L., Han J., Xiao M. M., Si J., Xu L., Qiu C. G., Peng L. M. Gigahertz Integrated Circuits Based on Carbon Nanotube Films. Nat. Electron. 2018, 1, 40.

[37] Tulevski G. S., Franklin A. D., Afzali A. High Purity Isolation and Quantification of Semiconducting Carbon Nanotubes via Column Chromatography. ACS Nano. 2013, 7, 2971– 2976.

[38] Kalbac M., Hsieh Y.-P., Farhat H., Kavan L., Hofmann M., Kong J., Dresselhaus M.S. Defects in Individual Semiconducting Single Wall Carbon Nanotubes: Raman Spectroscopic and in Situ Raman Spectroelectrochemical Study. Nano Letters. 2010, 10, 4619–4626.

[39] Xiao M., Liang S., Han J., Zhong D., Liu J., Zhang Z., Peng L. Batch Fabrication of Ultrasensitive Carbon Nanotube Hydrogen Sensors with Sub-ppm Detection Limit. ACS Sensors, 2018, 3, 749–756.

[40] Lucchese M. M., Stavale F., Ferreira E. H. M., Vilani C., Moutinho M. V. O., Capaz R. B., Achete C. A., Jorio A. Quantifying ion-induced defects and Raman relaxation length in graphene Carbon. 2010, 48, 5, 1592– 1597.

[41] Wang G. Density functional study on the increment of carrier mobility in armchair graphene nanoribbons induced by Stone–Wales defects Phys. Chem. Chem. Phys. 2011, 13, 11939-11944.

[42] Ma Y., Ma J. S., Lv Y. L., Liao J. N., Ji Y. Q., Bai H. C. Effect of Mono Vacancy Defect on the Charge Carrier Mobility of Carbon Nanotubes: A Case Study on (10, 0) Tube from First-principles. Superlattice. Microst. 2016, 99, 140-144.

[43] Kumar R., Aykol M., Cronin S.B. Effect of nanotube-nanotube coupling on the radial breathing mode of carbon nanotubes. Physical Review B. 2008,78.

[44] Sun Y., Wang Z., Wang W., Li G., Li P., Lian K., Zhang W., Zhuiykov S., Hu J., Chen L. Electrospinning preparation of Pd@Co_3O_4-ZnO composite nanofibers and their highly enhanced VOC sensing properties, Mater. Res. Bull. 2019, 109, 255–264.

[45] Liang Y.C., Liao W., Deng X.S. Synthesis and substantially enhanced gas sensing sensitivity of homogeneously nanoscale Pd- and Au-particle decorated ZnO nanostructures J. Alloy Compd. 2014, 599, 87-92.

[46] Hu J., Gao F.Q., Sang S.B., Li P.W., Deng X., Zhang W.D., Chen Y., Lian K. Optimization of Pd content in ZnO microstructures for high-performance gas detection J. Mater. Sci. 2015, 50, 1935-1942.

[47] Suhonen S, Valden M, Pessa M, Savimäki A, Härkönen M, Hietikko M, Pursiainen J, Laitinen R. Characterization of alumina supported Pd catalysts modified by rare earth oxides using X-ray photoelectron spectroscopy and X-ray diffraction: enhanced thermal stability of PdO in Nd/Pd catalysts. Appl Catal A. 2001, 207, 113–120.

[48] Hu J., Liu X., Zhang J., Gu X., Zhang Y. Plasmon-activated NO_2 sensor based on Au@MoS_2 core-shell nanoparticles with heightened sensitivity and full recoverability. Sens. Actuators, B. 2023, 382, 133505.

[49] Karmaoui M., Lajaunie L., Tobaldi D.M., Leonardi G., Benbayer C., Arenal R., Labrincha J.A., Neri G. Modification of anatase using noble-metals (Au, Pt, Ag): Toward a nanoheterojunction exhibiting simultaneously photocatalytic activity and plasmonic gas sensing. Appl. Catal. B Environ. 2017, 218, 370–384.

[50] Zhu H., Tao J., Dong X. Preparation and Photoelectrochemical Activity of Cr-Doped TiO_2 Nanorods with Nanocavities. J. Phys. Chem. C. 2010, 114, 2873–2879.

[51] Baidya T., Murayama T., Bera P., Safonova O.V., Steiger P., Katiyar N.K., Biswas K., Haruta M. Low-Temperature CO Oxidation over Combustion Made Fe- and Cr-Doped Co_3O_4 Catalysts: Role of Dopant's Nature toward Achieving Superior Catalytic Activity and Stability. J. Phys. Chem. C. 2017, 121, 15256–15265.

[52] Liang Y., Xiao M., Wu D., Lin Y., Liu L., He J., Zhang G., Peng L.-M., Zhang Z. Wafer-Scale Uniform Carbon Nanotube Transistors for Ultrasensitive and Label-Free Detection of Disease Biomarkers. ACS Nano. 2020, 14, 8866–8874.

[53] Murata Y., Starodub E., Kappes B.B., Ciobanu C.V., Bartelt N.C., Mccarty K.F., Kodambaka S. Orientation-dependent work function of graphene on Pd (111). Appl. Phys. Lett. 2010, 97, 143114.

[54] Prada S., Martinez U., Pacchioni G. Work function changes induced by deposition of ultrathin dielectric films on metals: A theoretical analysis. Physical Review B. 2008, 78.

[55] Aylward L.L., Barton H.A., Hays S.M. Biomonitoring Equivalents (BE) dossier for toluene. Regul. Toxicol. Pharmacol. 2008, 51, S27–S36.

[56] Hong Y.J., Yoon J.-W., Lee J.-H., Kang Y.C. One-Pot Synthesis of Pd-Loaded SnO_2 Yolk-Shell Nanostructures for Ultraselective Methyl Benzene Sensors. Chem. Eur. J. 2014, 20, 2737–2741.

[57] Hwang S.-J., Choi K.-I., Yoon J.-W., Kang Y.C., Lee J.-H. Pure and Palladium-Loaded Co_3O_4 Hollow Hierarchical Nanostructures with Giant and Ultraselective Chemiresistivity to Xylene and Toluene. Chem. Eur. J. 2015, 21, 5872–5878.

[58] Ma H., Xu Y.M., Rong Z.M., Cheng X.L., Gao S., Zhang X.F., Zhao H., Huo L.H. Highly toluene sensing performance based on monodispersed Cr_2O_3 porous micro spheres, Sens. Actuators. B. 2012, 174, 325–331.

[59] Yoon J.-W., Hong Y.J., Park G.D., Hwang S.-J., Abdel-Hady F., Wazzan A.A., Kang Y.C., Le J.-H. Kilogram-scale synthesis of Pd-Loaded quintuple-shelled Co_3O_4 microreactors and their application to ultrasensitive and ultraselective detection of methylbenzenes. ACS Appl. Mater. Interfaces. 2015, 7, 7717-7723.

[60] Kim B.-Y., Ahn J.H., Yoon J.-W., Lee C.-S., Kang Y.C., Abdel-Hady F., Wazzan A.A., Lee J.-H. Highly selective xylene sensor based on $NiO/NiMoO_4$ nanocomposite hierarchical spheres for indoor air monitoring. ACS Appl. Mater. Interfaces. 2016, 8, 34603-34611.

[61] Lundström I., Sundgren H., Winquist F., Eriksson M., Krantz-Rülcker C., Lloyd-Spetz A. Twenty-five years of field effect gas sensor research in Linköping. Sens. Actuators B Chem. 2007, 121, 247-262.

[62] Hong S., et al., FET-type gas sensors: a review. Sens. Actuators B Chem. 2021, 330, 129240.

[63] Yamazoe N., Fuchigami J., Kishikawa M., Seiyama T. Interactions of tin oxide surface with O_2, H_2O and H_2. Surf. Sci. 1979, 86, 335-344.

[64] Lenaerts S, Roggen J, Maes G. FT-IR characterization of tin dioxide gas sensor materials under working conditions. Spectrochim. Acta A Mol. Biomol. Spectrosc. 1995, 51, 5, 883-894.

[65] Sun Y., Wang Z., Wang W., Li G., Li P., Lian K., Zhang W., Zhuiykov S., Hu J., Chen L. Electrospinning preparation of $Pd@Co_3O_4$-ZnO composite nanofibers and their highly enhanced VOC sensing properties, Mater. Res. Bull. 2019, 109, 255–264.

[66] Zhang M., Zhen Y., Sun F., Xu C. Hydrothermally synthesized SnO_2-graphene composites for H_2 sensing at low operating temperature Mat Sci Eng B Adv. 2016, 209, 37-44.

[67] Hong Y.J., Yoon J.-W., Lee J.-H., Kang Y.C. One-Pot Synthesis of Pd-Loaded SnO_2 Yolk-Shell Nanostructures for Ultraselective Methyl Benzene Sensors. Chem. Eur. J. 2014, 20, 2737–2741.

[68] Oprea A., Barsan N., Weimar U. Work function changes in gas sensitive materials: Fundamentals and applications, Sens. Actuators B Chem. 2009, 142, 470–493.

612 [69] Inaba A., Yoo G., Takei Y., Matsumoto K., Shimoyama I. A graphene FET gas sensor gated
613 by ionic liquid, IEEE, 2013, 2013, 969-972.